Electronic Supplementary Material (ESI) for Dalton Transactions.

Supporting Information

Effect of *f*-*f* Interactions on the Quantum Tunnelling of the Magnetization: Mono- and Dinuclear Dy(III) Phthalocyaninato Triple-Decker Single-Molecule Magnets with the Same Octacoordination Environment

Keiichi Katoh, Rina Asano, Akira Miura, Yoji Horii, Takaumi Morita, Brian K. Breedlove, and Masahiro Yamashita**

Table of Contents

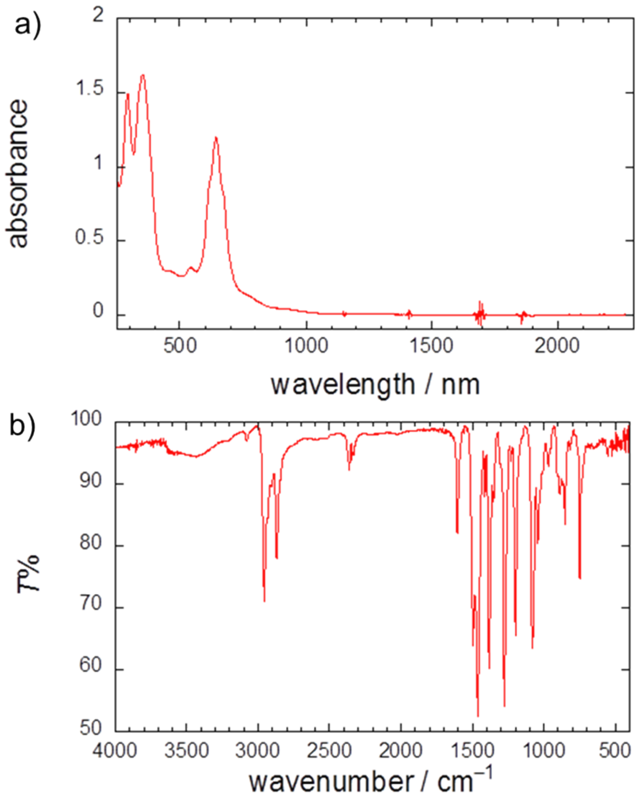

Figure S1. a) Electronic spectra of **1** in $CHCl_3$ (~10^{-5} M) at 298 K. b) FT-IR spectra of **1** as KBr pellets at 298 K.

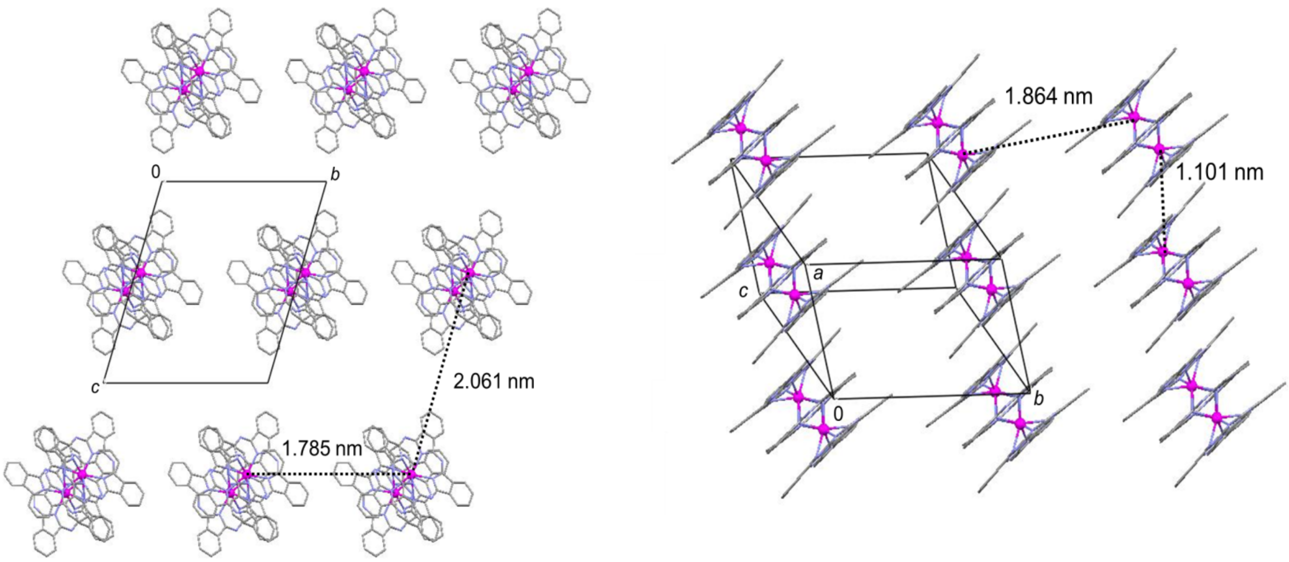

Figure S2. Packing diagram of **1**. EtOH located between the *n*-butoxy chains were omitted for clarity.

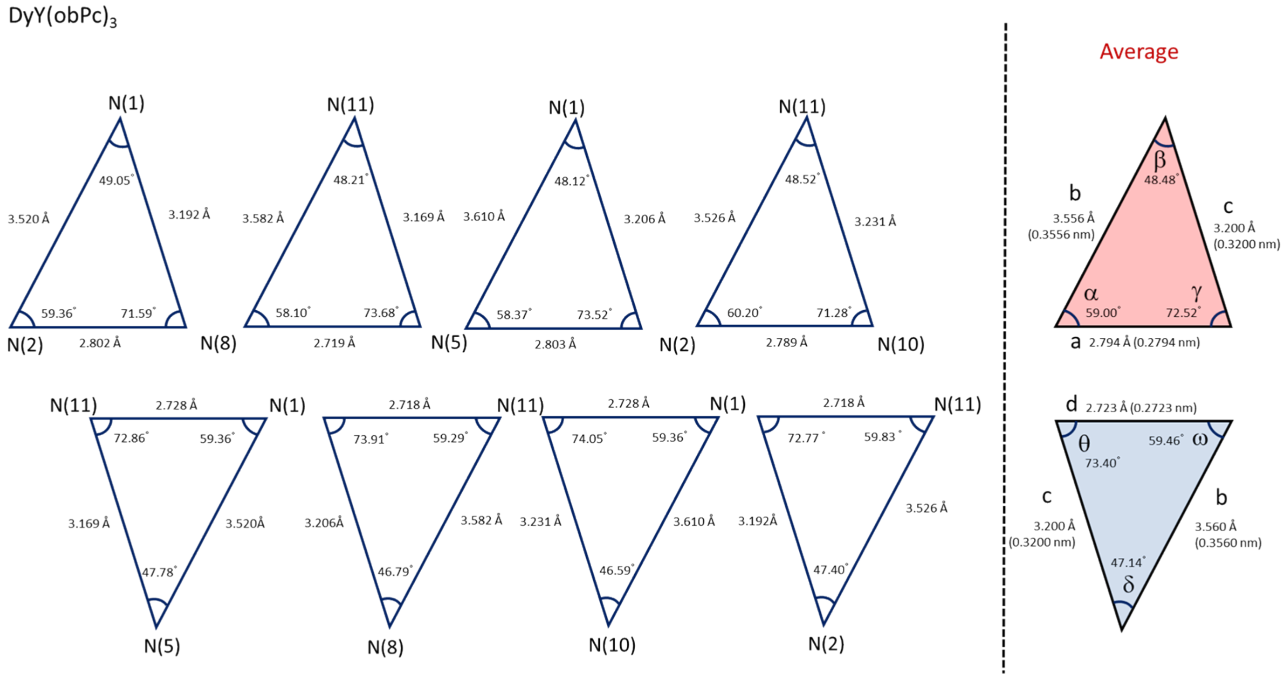

Figure S3-1. Schematic illustration (distance and angles) of the square-antiprismatic coordination site in the multiple-decker Dy(III)-Pc systems: $DyY(obPc)_3$ (**1**).

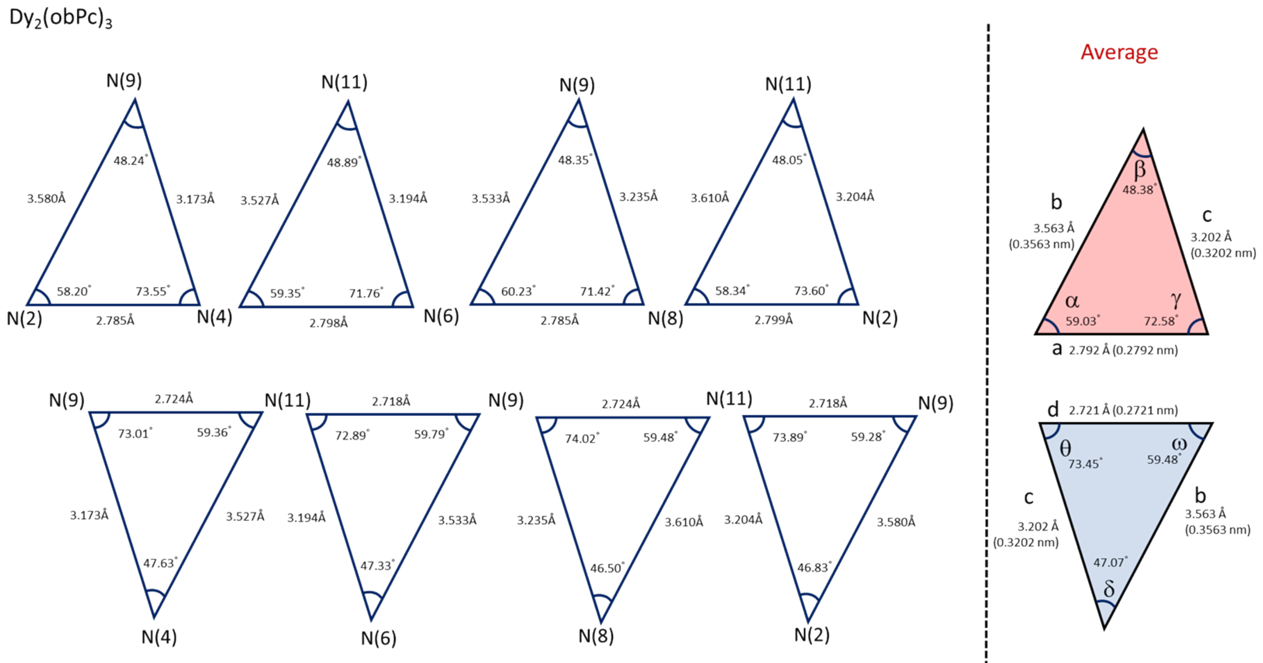

Figure S3-2. Schematic illustration (distance and angles) of the square-antiprismatic coordination site in the multiple-decker Dy(III)-Pc systems: $Dy_2(obPc)_3$ (**2**).

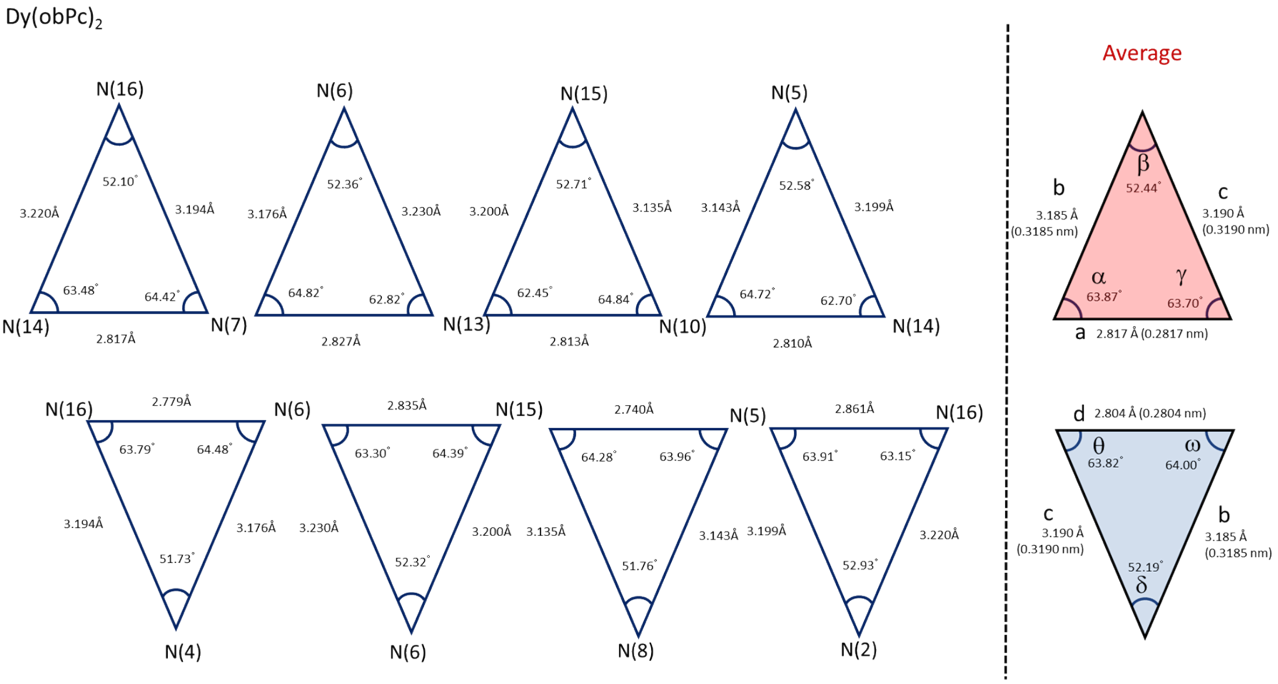

Figure S3-3. Schematic illustration (distance and angles) of the square-antiprismatic coordination site in the multiple-decker Dy(III)-Pc systems: Dy(obPc)$_2$.

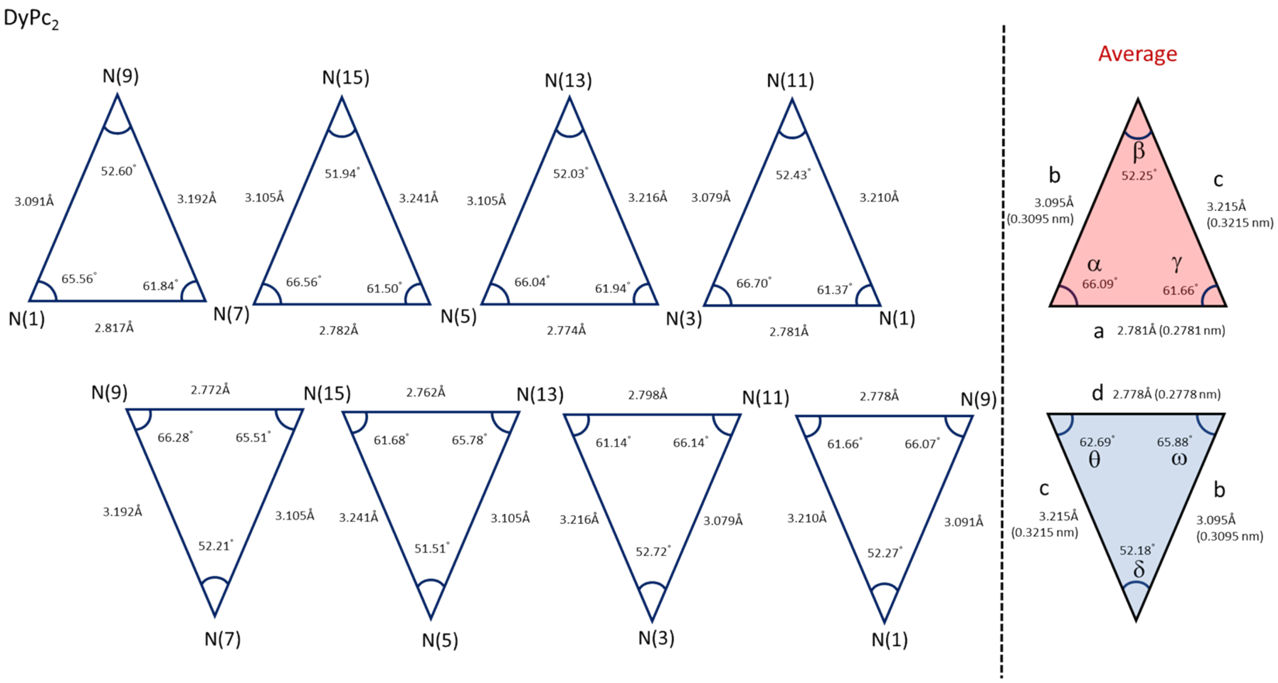

Figure S3-4. Schematic illustration (distance and angles) of the square-antiprismatic coordination site in the multiple-decker Dy(III)-Pc systems: DyPc$_2$.

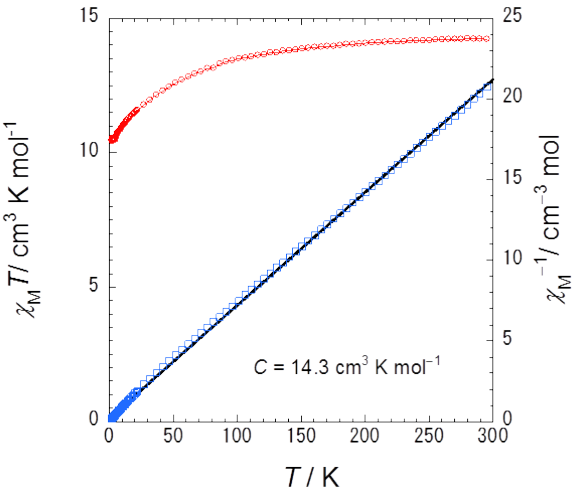

Figure S4. Temperature (T) dependence of $\chi_M T$ and χ_M^{-1} for powder samples of **1** in a field of 1000 Oe. In the χ_M^{-1} versus T plot, the black solid line represents a linear fit of all data.

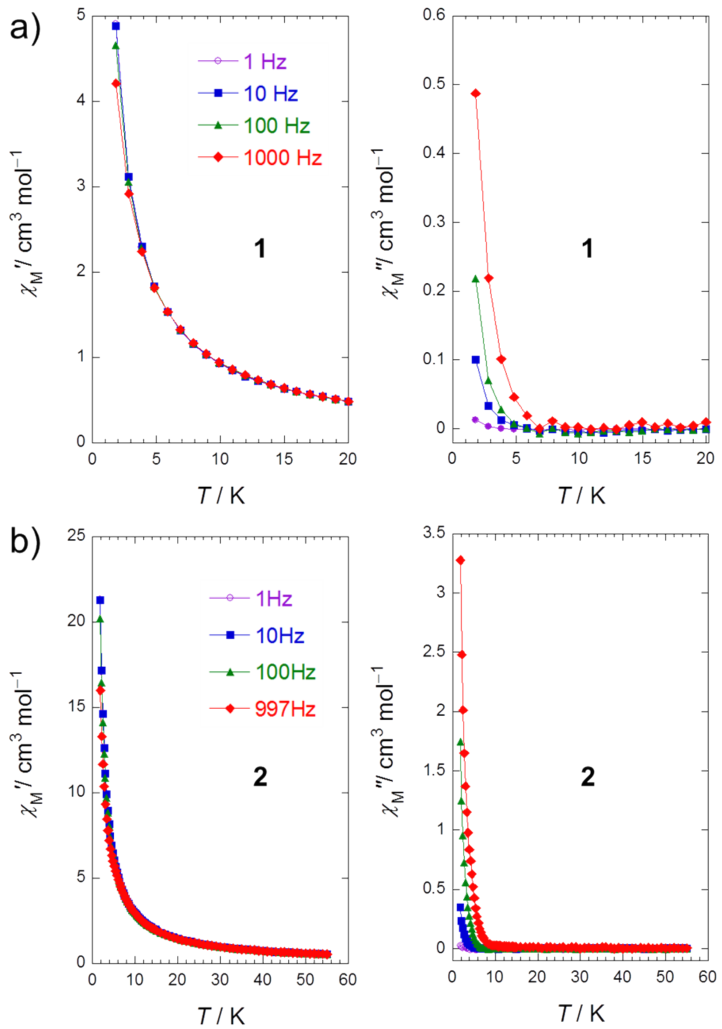

Figure S5. a) Frequency (ν) and temperature (T) dependences of the ac magnetic susceptibility in-phase (χ_M') and out-of-phase (χ_M'') of a) **1** and b) **2** at zero dc field.

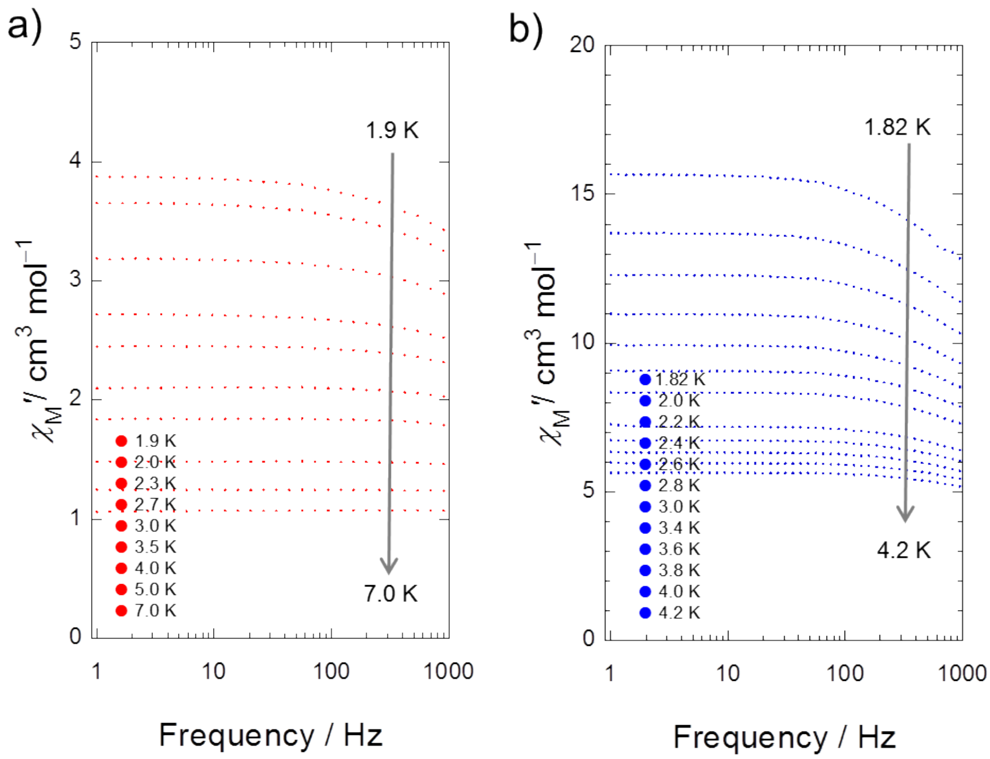

Figure S6. Temperature (T) and frequency (ν) dependent of the ac measurements (χ_M' versus ν plots) of **1** and **2** in a zero dc field.

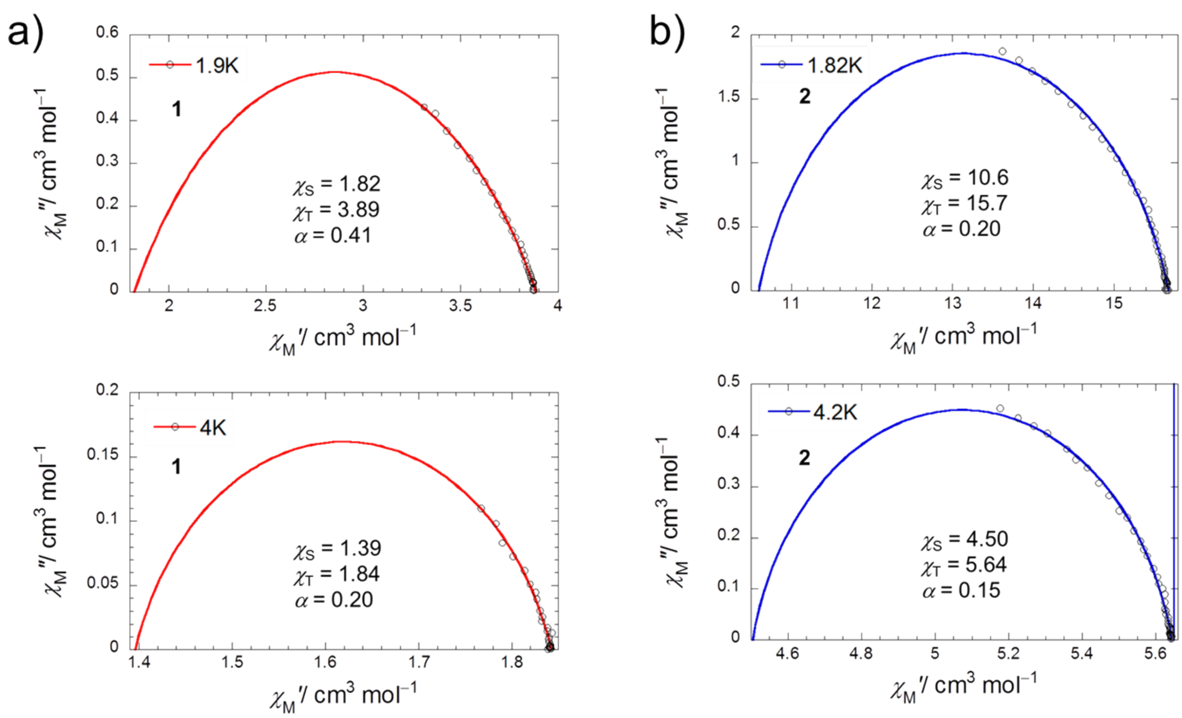

Figure S7. Selected Argand plots (χ_M'' versus χ_M' plots) in a zero dc field for a) **1** and b) **2**. Solid lines (red and blue) were fitted by using a generalized Debye model (eq. 4).

Table S1. These parameters in **1** were obtained from fittings using a generalized Debye model

T / K	χ_S	χ_T	α	τ / s
1.9	1.82	3.89	0.41	3.20×10^{-5}
2.0	1.66	3.67	0.42	3.10×10^{-5}
2.3	1.59	3.19	0.39	3.11×10^{-5}
2.7	1.09	2.72	0.41	3.42×10^{-5}
3.0	1.36	2.45	0.33	2.96×10^{-5}
3.5	1.39	2.11	0.29	3.42×10^{-5}
4.0	1.39	1.84	0.20	3.49×10^{-5}

Table S2. These parameters in **2** were obtained from fittings using a generalized Debye model

T / K	χ_S	χ_T	α	τ / s
1.82	10.60	15.70	0.20	1.30×10^{-4}
2.0	8.51	13.70	0.24	1.30×10^{-4}
2.2	7.90	12.30	0.23	1.29×10^{-4}
2.6	6.72	9.94	0.22	1.26×10^{-4}
2.8	6.29	9.07	0.21	1.25×10^{-4}
3.0	5.92	8.35	0.20	1.24×10^{-4}
3.4	4.78	7.22	0.29	1.14×10^{-4}
3.6	7.98	6.74	0.19	1.11×10^{-4}
3.8	4.67	6.33	0.21	1.11×10^{-4}
4.0	4.48	5.97	0.20	1.13×10^{-4}
4.2	4.50	5.64	0.15	1.06×10^{-4}

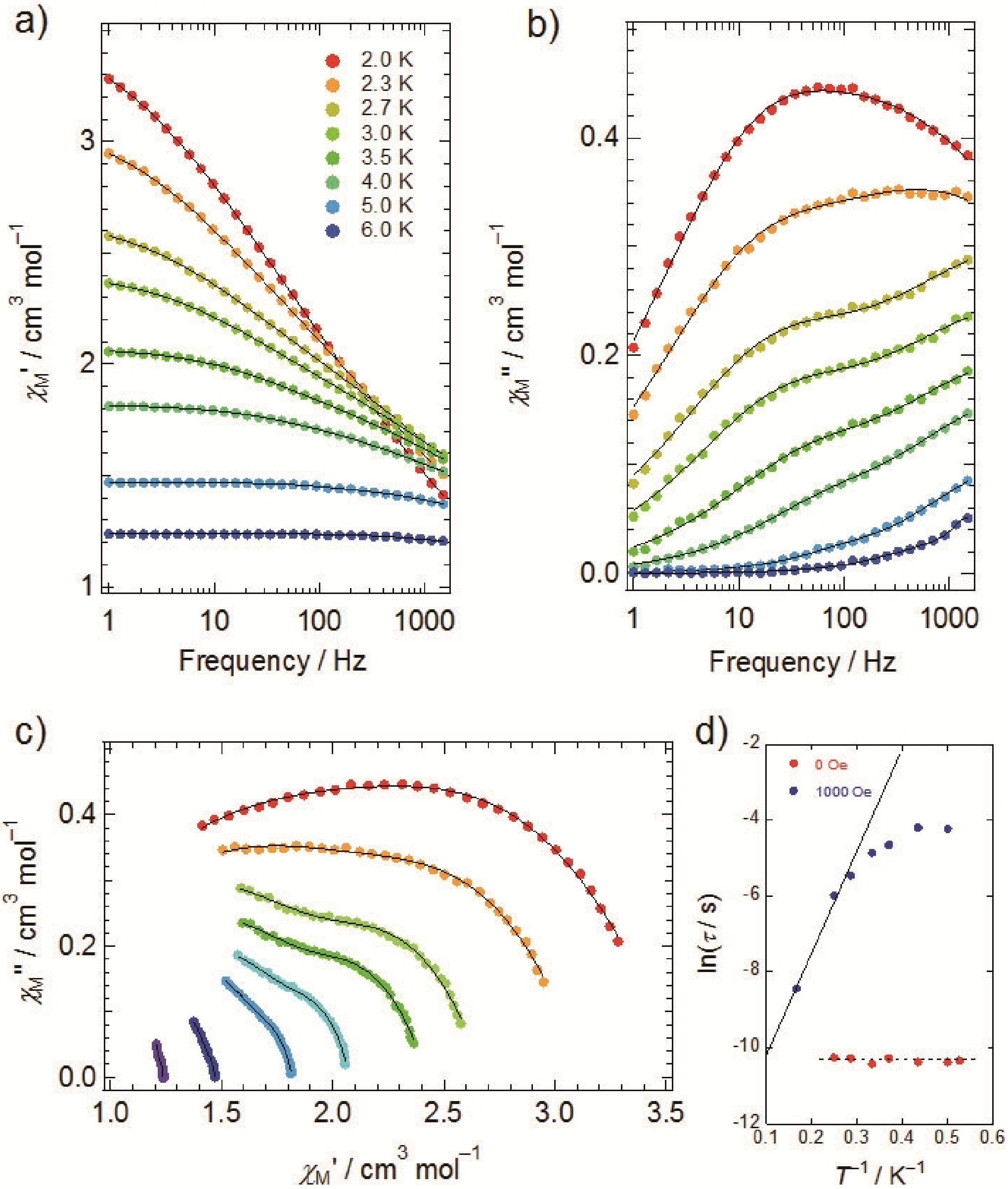

Figure S8. Temperature (T) and frequency (ν) dependences of the ac susceptibilities of **1** in a dc field of 1000 Oe. a) χ_M' versus ν plots, b) χ_M'' versus ν plots, and c) Argand plot. Black solid lines were fitted by using an extended Debye model. d) Arrhenius plot for **1** in a dc field of 1000 Oe. The solid lines were fitted using least-square analysis on the data in the high-T region using the equation $\tau = \tau_0 \exp(\Delta/k_B T)$ with the kinetic parameters (Δ/hc = 18 cm, $\tau_0 = 3.1 \times 10^{-6}$ s).

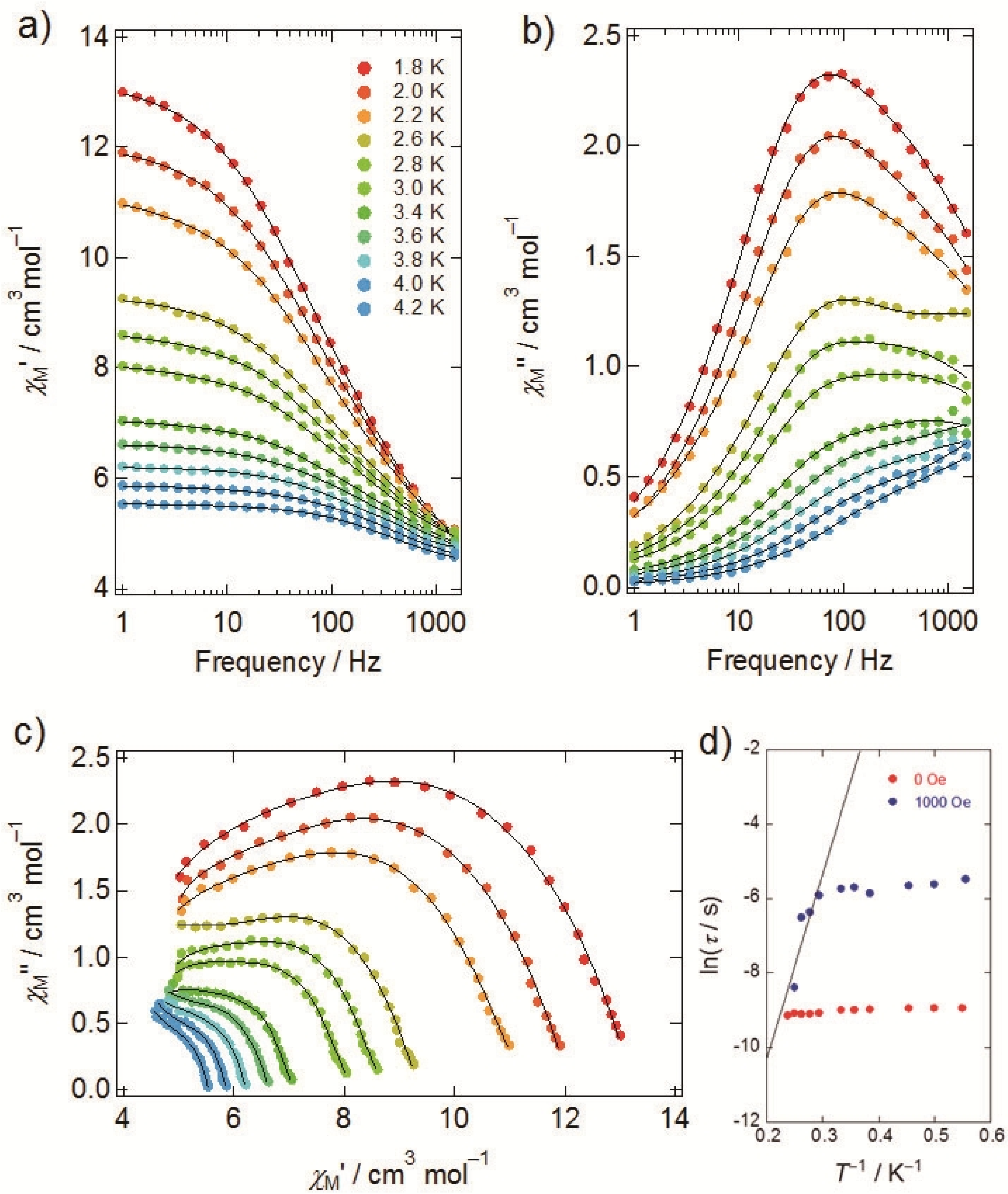

Figure S9. Temperature (T) and frequency (ν) dependences of the ac magnetic susceptibilities of **2** in an H_{dc} of 1000 Oe. a) χ_M' versus ν plots, b) χ_M'' versus ν plots, and c) Argand plot. Black solid lines were fitted by using an extended Debye model. d) Arrhenius plot for **2** in an H_{dc} of 1000 Oe. The solid lines were fitted by using least-square analysis on the data in the high T region with the equation $\tau = \tau_0\exp(\Delta/k_BT)$, and the kinetic parameters (Δ/hc = 35 cm, $\tau_0 = 1.3 \times 10^{-5}$ s).

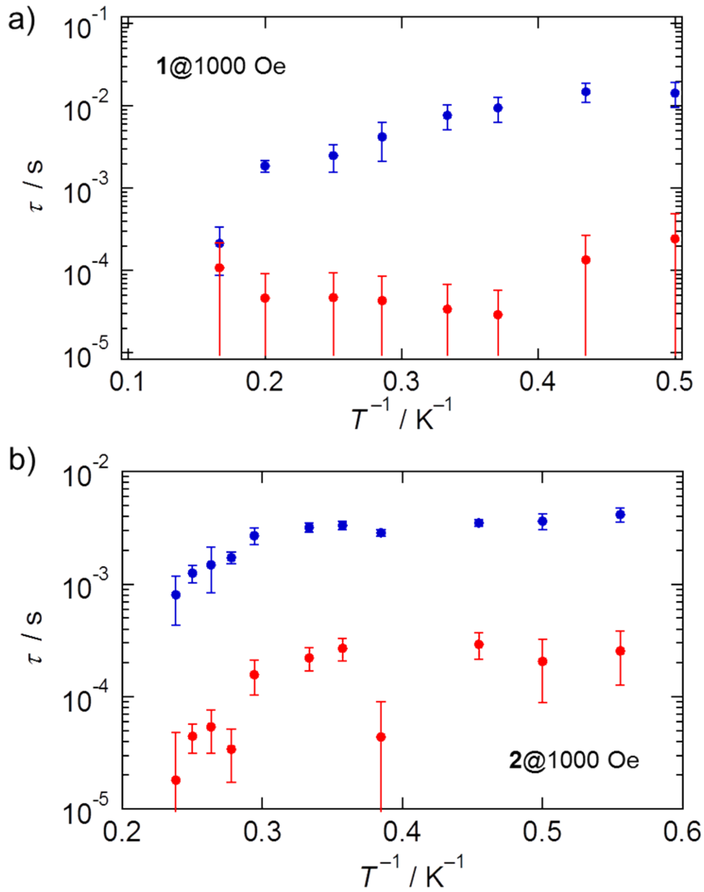

Figure S10. Arrhenius plots made by using parameters obtained from the χ_M'' versus ν plots (Figures 10b and 11b) for a) **1** and b) **2** in a dc magnetic field of 1000 Oe. Red circles indicate the residual quantum regime, which have a large margin of error. Therefore, these data cannot be used for discussions (see main text).

Extended Debye Model: In order to understand the different relaxation mechanisms corresponding to the two observed peaks, an extended Debye model (eq. 5) was used to fit τ_1 and τ_2:

$$\chi_{total}(\omega) = \chi_s + (\chi_T - \chi_S)\left[\frac{\beta}{1+(i\omega\tau_1)^{1-\alpha_1}} + \frac{1-\beta}{1+(i\omega\tau_2)^{1-\alpha_2}}\right] \tag{5}$$

where χ_S is the adiabatic susceptibility, χ_T is the isothermal susceptibility, ω (= $2\pi f$) is the angular frequency, τ_1 and τ_2 are the magnetization relaxation times, τ_1 and τ_2 describe the distributions of the relaxation processes, β is the weight of the first relaxation process, and $(1-\beta)$ corresponds to the second one. The real part and the imaginary part are given by eqs. 6 and 7, respectively.

$$\chi' = \chi_S + (\chi_T - \chi_S)\left\{\frac{\beta\left[1 + (\omega\tau_1)^{1-\alpha_1} sin^1/_2\alpha_1\pi\right]}{1 + 2(\omega\tau_1)^{1-\alpha_1} sin^1/_2\alpha_1\pi + (\omega\tau_1)^{2(1-\alpha_1)}} + \frac{(1-\beta)\left[1 + (\omega\tau_2)^{1-\alpha_2} sin^1/_2\alpha_2\pi\right]}{1 + 2(\omega\tau_2)^{1-\alpha_2} sin^1/_2\alpha_2\pi + (\omega\tau_2)^{2(1-\alpha_2)}}\right\} \tag{6}$$

$$\chi'' = (\chi_T - \chi_S)\left\{\frac{\beta(\omega\tau_1)^{1-\alpha_1} cos^1/_2\alpha_1\pi}{1 + 2(\omega\tau_1)^{1-\alpha_1} sin^1/_2\alpha_1\pi + (\omega\tau_1)^{2(1-\alpha_1)}} + \frac{(1-\beta)(\omega\tau_2)^{1-\alpha_2} cos^1/_2\alpha_2\pi}{1 + 2(\omega\tau_2)^{1-\alpha_2} sin^1/_2\alpha_2\pi + (\omega\tau_2)^{2(1-\alpha_2)}}\right\} \tag{7}$$

To elucidate the details of the H_{dc} dependence of **1**, the ν dependence of χ_M' and χ_M'' signals in the range of 1–1488 Hz were measured in an H_{dc} of 1000 Oe (Figures S6a–c). Below 6 K, however, the behavior deviated from that for a single relaxation process. Thus, we concluded that the relaxation process was a mixture of QTM processes in the low-T region. It is possible to suppress QTM by applying an H_{dc}, but it cannot be completely suppressed. Therefore, in order to separate the two relaxation processes, we analysed the data by using an extended Debye model (eq. 5–7) to extract τ (Figure S8a–c). One of the two τ values has a large margin of error. This is a QTM component, which is not completely suppressed by applying an H_{dc}. Δ/hc was estimated to be 18 cm^{-1} with $\tau_0 = 3.1 \times 10^{-6}$ s from an Arrhenius plot for **1** in the T range of 2–6 K in an H_{dc} of 1000 Oe (Figure S8d). The values of Δ/hc and τ_0 are on the same order of magnitude as those for the Dy(III)-Pc double-decker complexes. These results confirm that the QTM process is suppressed by applying an H_{dc}, indicating a thermal relaxation process. These phenomena have been observed for **2** in an H_{dc} of 1000 Oe (Figures S9a–c). Δ/hc was estimated to be 35 cm^{-1} with $\tau_0 = 1.3 \times 10^{-9}$ s from the Arrhenius plot in Figures S9d and S8b. However, these results confirm that the QTM process is not completely suppressed by applying an H_{dc} of 1000 Oe, indicating that a QTM process occurs for $T < 3$ K.